

DOI: 10.46698/VNC.2026.27.54.001

Original paper

# Hypocenter distribution of volcanic earthquakes beneath Mount Sinabung (Oct 2023–Apr 2024) using an adaptive damping Geiger relocation

E. Minarto<sup>1</sup>, A. Ditaningrum<sup>1</sup>, Kristianto<sup>2</sup>

<sup>1</sup> Sepuluh Nopember Institute of Technology, Department of Physics,  
Surabaya 60111, Indonesia,  
e-mail: eko.minarto@its.ac.id, arfi.dita@gmail.com;

<sup>2</sup> Center for Volcanology and Geological Disaster Mitigation (PVMBG),  
57 J. Diponegoro Str., Bandung 40122, Indonesia, e-mail: kristianto02@gmail.com

Received: 29.10.2025, revised: 10.02.2026, accepted: 12.02.2026

**Abstract: Relevance.** Mount Sinabung has remained one of the most active volcanoes in Indonesia during the past decade, producing recurrent seismic swarms that reflect dynamic subsurface processes. Understanding the spatial distribution of hypocenters is critical for constraining magma transport pathways and assessing volcanic hazards in densely populated regions. **The aim** of this study is to refine the earthquake catalogue for Sinabung by relocating events with improved accuracy, thereby distinguishing shallow brittle-failure processes from deeper magmatic activity. We analyzed 61 volcanic earthquakes recorded between October 2023 and April 2024. Hypocenter relocation was performed using a Geiger least-squares algorithm with adaptive damping, designed to minimize instability in heterogeneous velocity structures. **Methods.** To evaluate robustness, we applied  $\pm 10\%$  P-wave velocity sensitivity tests and jackknife resampling of seismic stations. These procedures allowed us to identify well-constrained events and flag model-sensitive cases requiring cautious interpretation. **The results** reveal two distinct hypocenter populations. Shallow VTB events (0.3–2.0 km depth) occur as semi-continuous swarms beneath the summit and upper flanks, consistent with near-surface brittle failure or hydrothermal cracking. In contrast, deeper VTA events (2.5–14 km depth) form several aligned clusters rather than a single source, delineating vertically segmented pathways coherent with conduit structures or mid-crustal magma transport. Epicenters are concentrated within 0–5 km of the summit, highlighting a vertically continuous but segmented plumbing system. These findings provide new constraints on the geometry of magma pathways beneath Sinabung and contribute to improved models of volcanic hazard assessment in northern Sumatra.

**Keywords:** Mount Sinabung, volcanic earthquake, hypocenter, Geiger method, seismic monitoring.

**Acknowledgements:** We thank PVMBG Bandung for providing seismic data and station metadata. We acknowledge technical assistance with picking and processing from colleagues in the Department of Physics, Sepuluh Nopember Institute of Technology. This research received no external funding.

**For citation:** Minarto E., Ditaningrum A., Kristianto. Hypocenter distribution of volcanic earthquakes beneath Mount Sinabung (Oct 2023–Apr 2024) using an adaptive damping Geiger relocation. *Geologiya i Geofizika Yuga Rossii = Geology and Geophysics of Russian South*. (in Russ.). 2026. 16(1): 93-108. DOI: 10.46698/VNC.2026.27.54.001

УДК 550.34; 551.21

DOI: 10.46698/VNC.2026.27.54.001

Оригинальная статья

Распределение гипоцентров вулканических  
землетрясений под горой Синабунг  
(октябрь 2023 г. – апрель 2024 г.)  
с использованием адаптивного демпфирования  
по методу перемещения Гейгера

Э. Минарто<sup>1</sup>, А. Дитанингрум<sup>1</sup>, Кристианто<sup>2</sup>

<sup>1</sup> Институт технологий Сепулук Нопембер, факультет физики, Индонезия, 60111, г. Сурабая, e-mail: eko.minarto@its.ac.id, arfi.dita@gmail.com;

<sup>2</sup> Центр вулканологии и смягчения геологических опасностей, Индонезия, 40122, г. Бандунг, ул. Дж. Дипонегоро, 57, e-mail: kristianto02@gmail.com

Статья поступила: 29.10.2025, доработана: 10.02.2026, принята к публикации: 12.02.2026

**Резюме: Актуальность работы.** Вулкан Синабунг остается одним из наиболее активных вулканов Индонезии в течение последнего десятилетия, порождая повторяющиеся рои землетрясений, которые отражают динамические процессы в недрах. Понимание пространственного распределения гипоцентров имеет критическое значение для определения путей транспорта магмы и оценки вулканической опасности в густонаселенных регионах. **Цель данного исследования** – уточнить каталог землетрясений для Синабунга путем переопределения локации событий с повышенной точностью, что позволит различить процессы неглубокого хрупкого разрушения от более глубокой магматической активности. Было проанализировано 61 вулканическое землетрясение, зарегистрированное в период с октября 2023 по апрель 2024 года. **Методы.** Переопределение гипоцентров выполнялось с использованием алгоритма Гейгера по методу наименьших квадратов с адаптивным демпфированием, разработанного для минимизации нестабильности в неоднородных скоростных структурах. Для оценки надежности были применены тесты на чувствительность к  $\pm 10\%$  изменению скорости Р-волн и процедура jackknife-ресэмплинга сейсмических станций. Эти процедуры позволили выявить хорошо определяемые события и отметить чувствительные к модели случаи, требующие осторожной интерпретации. **Результаты.** Результаты выявили две различные популяции гипоцентров. Мелкие события типа VTB (глубина 0,3–2,0 км) образуют почти непрерывные рои под вершиной и верхними склонами, что согласуется с процессами хрупкого разрушения вблизи поверхности или гидротермального растрескивания. В отличие от них, более глубокие события типа VTA (глубина 2,5–14 км) формируют несколько выстроенных в линию кластеров, а не единый источник, очерчивая вертикально сегментированные пути, соответствующие структурам проводящего канала или транспорту магмы в средней коре. Эпицентры сконцентрированы в пределах 0–5 км от вершины, что указывает на вертикально непрерывную, но сегментированную магмоподводящую систему. Эти результаты дают новые ограничения на геометрию магматических путей под Синабунгом и способствуют совершенствованию моделей оценки вулканической опасности на севере Суматры.

**Ключевые слова:** вулкан Синабунг, вулканическое землетрясение, гипоцентр, метод Гейгера, сейсмический мониторинг.

**Благодарности:** Авторы благодарят Центр вулканологии и смягчения последствий геологических катастроф (PVMBG, Бандунг) за предоставление сейсмических данных и метаинформации о станциях. Мы также признательны коллегам с кафедры физики Технологического института «Сепулух Нопембер» за техническую помощь в отборе и обработке данных. Данное исследование не получало внешнего финансирования.

**Для цитирования:** Минарто Э., Дитанингрум А., Кристианто. Распределение гипоцентров вулканических землетрясений под горой Синабунг (октябрь 2023 г. – апрель 2024 г.) с использованием адаптивного демпфирования по методу перемещения Гейгера. *Геология и геофизика Юга России*. 2026. 16(1): 93-108. DOI: 10.46698/VNC.2026.27.54.001

## Introduction

This study implements a rigorously parameterized Geiger relocation workflow with adaptive damping to refine volcano-proximal seismic data from Mount Sinabung (October 2023–April 2024). The approach yields a reproducible, sensitivity-annotated hypocenter catalogue. In contrast to earlier relocations, we employ manually curated P- and S-wave picks with explicit numeric weighting and adaptive damping protocols. Each event is tested with  $\pm 10\%$  P-wave velocity perturbations, station jackknife displacement metrics, and covariance estimates to evaluate stability. Conversion scripts and GAD control files are archived to ensure exact reproducibility. These enhancements improve the interpretability of depth classifications, confirm the robustness of a February 2024 deep event under multiple perturbations, and provide operational guidance to PVMBG on station densification strategies and relocation threshold calibration.

Indonesia occupies a complex plate-boundary zone at the junction of the Eurasian, Pacific and Indo-Australian plates [Charlton, 2000], forming a highly active segment of the Pacific Ring of Fire where sustained subduction and related crustal deformation generate prolific magmatism and frequent seismicity. This tectonic setting produces 127 historically active volcanoes distributed across Java, Nusa Tenggara, Bali, Sulawesi, Sumatra and adjacent islands [Hariyono, Liliyasi, 2018], many of which are monitored continuously by the Center for Volcanology and Geological Hazard Mitigation (PVMBG) because of their hazard potential. Mount Sinabung (North Sumatra) is one such monitored system; its eruptive episodes and associated seismic unrest are readily characterized using standard seismological workflows, including manual P- and S-arrival picking and iterative relocation algorithms (e.g., Geiger least-squares), which yield the hypocentral precision required to resolve magma-related seismicity and migration pathways beneath the edifice [Annisa et al., 2021]. Although convergent (subduction) processes are the principal driver of arc volcanism in Indonesia, local extensional and transform strain components modulate crustal fracture networks and fluid pathways that focus magma ascent and control the spatial distribution of volcanic seismicity [O’Har, Karlstrom, 2023].

Mount Sinabung is an andesitic stratovolcano [Gunawan, et al., 2019] in the Karo Highlands, North Sumatra, Indonesia (Fig. 1). After a prolonged quiescence the volcano reactivated in 2010 and has produced repeated eruptive episodes, with notable pulses in 2013–2014 and further activity through 2016 and 2021. Its proximity to populated areas and the frequent occurrence of shallow volcanic earthquakes make Sinabung a priority for continuous monitoring; seismic observations are central to tracking subsurface processes such as magma migration, pressurization of hydrothermal systems, and fracturing associated with volcanic unrest [Nakada et al., 2019].

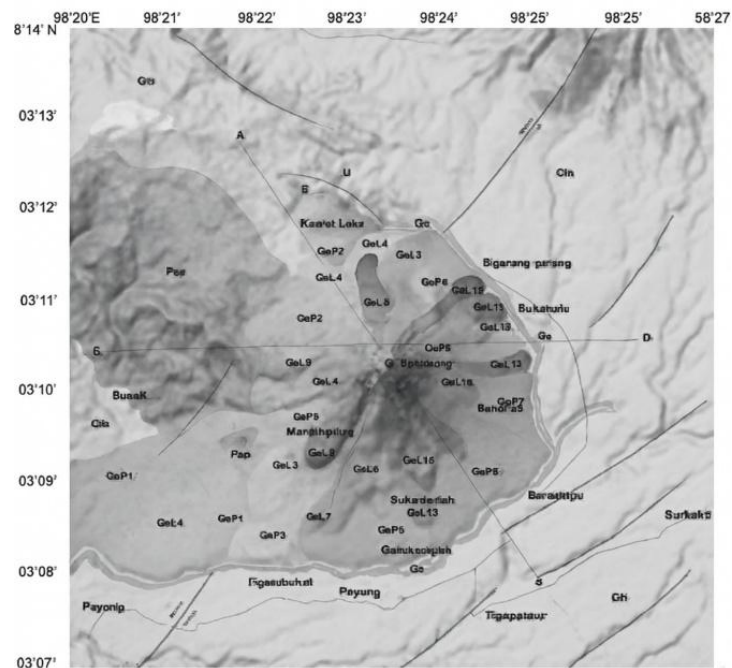


Fig. 1. Geological map of Mount Sinabung

Accurate determination of hypocenter distributions beneath Sinabung provides crucial constraints on shallow magma and fluid pathways, faulting within the volcanic plumbing system, and the depth ranges over which seismic energy is released [Kusumo et al., 2025]. These constraints are directly relevant to hazard assessment and mitigation because they help distinguish shallow hydrothermal or fracture-related seismicity from deeper magmatic signals that may precede eruptive behavior. Locating volcanic earthquakes is challenging: events are typically shallow and emergent, pick uncertainties are larger than for tectonic earthquakes, and results are sensitive to local station geometry and velocity-model assumptions.

The Geiger iterative travel-time inversion remains a widely used and computationally efficient method for routine earthquake location [Karasozen, Karasozen, 2020]. Modern implementations that incorporate stabilizing measures such as adaptive damping reduce non-physical jumps and improve convergence in sparse or noisy networks, yielding more robust hypocenter clouds for volcanic settings. Building on previous relocations at Sinabung [Sutawidjaja et al., 2013], this study applies the Geiger iterative least-squares method with adaptive damping (GAD) to earthquakes recorded between October 2023 and April 2024. We classify events by depth, present detailed spatial and depth distributions, quantify location quality and sensitivity, and compare our results with earlier studies to draw implications for operational monitoring and near-field hazard mitigation.

Disaster mitigation minimizes the adverse consequences of hazards through a combination of preparedness and long-term risk-reduction measures [Senathirajah et al., 2023]. Mitigation interventions may be implemented before, during, or after an event; under Law No. 24 of 2007, actions at any of these stages are recognized as mitigation. Preparedness comprises proactive activities that reduce vulnerability and strengthen response capacity, including public information campaigns and the dissemination of clear evacuation routes and rescue procedures to ensure timely and effective action during emergencies [Bakhshian, Martinez-Pastor, 2023].

## Data

### Network and instruments

Seismic data were obtained from a local network of seven broadband and short-period stations operated by PVMBG Bandung and deployed around Mount Sinabung to maximize azimuthal coverage of the edifice. Metadata for each station, including code, coordinates, elevation, sensor type, and sampling rate, are summarized in Table 1. Station siting prioritized low-noise environments on competent ground, with reliable power and telemetry to enable near real-time data transfer. Sensor orientation and installation depth followed PVMBG standards to minimize environmental and cultural noise. Timing at all stations was synchronized to GPS clocks and verified through routine metadata audits, ensuring sub-millisecond accuracy required for robust travel-time based location and relocation analyses.

Table 1

Station code, latitude, longitude, elevation, sensor type, and sampling rate<sup>a</sup>

Station Name/ code	Latitude (°N)	Longitude (°E)	Elevation (m)	Sensor type	Sampling rate (Hz)
Sukanalu SKN	3.1700	98.3920	1200	Broadband (STS-2)	100
Lau Kawar LKW	3.1805	98.3850	950	Short-period (2 Hz)	100
Gamber GBR	3.1580	98.4015	1350	Broadband (CMG-3T)	100
Sibayak SBY	3.1900	98.4100	1100	Short-period (1 Hz)	100
Mardinding MDD	3.1625	98.3760	900	Broadband (Trillium 120)	100
Kebayaken KBY	3.1755	98.4055	1400	Short-period (2 Hz)	200
Sigarang-Garang SGR	3.1500	98.3890	1000	Broadband (STS-2)	100

Recording instrumentation comprised a mix of broadband sensors (for low-frequency energy and waveform completeness) and high-gain short-period sensors (for improved signal-to-noise on emergent volcanic phases), digitized at sampling rates listed in Table 1. Before relocation, continuous records were visually inspected and subjected to automated quality control: instrument response removal, bandpass filtering tailored to expected P- and S-phase frequency content, and manual or semi automatic pick review to flag low-quality or ambiguous arrivals. We quantified station sensitivity and azimuthal coverage, and we evaluated network performance metrics (detection completeness, pick residual distributions) to inform data weighting and damping choices in the Geiger iterative inversion, following best practice recommendations for optimizing hypocenter resolution in small, volcano-focused networks.

### Recording period and picks

Continuous waveform records from 1 October 2023 to 30 April 2024 were inspected in Swarm to compile a high-quality arrival dataset. Traces were reviewed station-by-station with variable time windows to capture both isolated and clustered events, while spectral and time-domain displays aided identification of emergent phases and suppression of

coherent noise. Narrow-band filtering (1–10 Hz for short-period volcanic phases; 0.5–5 Hz for broadband low-frequency signals) ensured consistent phase recognition across the network.

P and S arrival times were picked manually to maximise consistency and to avoid systematic bias introduced by automatic pickers in low signal-to-noise situations [Kato et al., 2025]. Each pick record includes the station code, phase identifier (P or S), UTC pick time, and a discrete pick-quality flag. Pick quality was assigned on a three-tier scale: high (clear first arrival, uncertainty  $\leq 0.02$  s), medium (moderately emergent or low SNR, uncertainty 0.02–0.1 s), and low (ambiguous or strongly emergent, uncertainty  $> 0.1$  s). Picks flagged as low quality were retained in the master file for completeness but down-weighted in subsequent inversion and sensitivity analyses.

Arrival picks were exported from Swarm as Arrival.dat and converted to the Geiger adaptive damping (GAD) input format using a reproducible conversion script. The conversion step verified station codes against the metadata table, standardized time stamps to ISO-8601 UTC, and propagated the pick-quality flags into the GAD weighting scheme. Prior to inversion, we performed a final quality control pass that removed obvious outliers, corrected inconsistent station polarity or phase labels, and ensured that each event had a minimum of four high- or medium-quality picks. This conservative selection protocol underpins the robustness and interpretability of the relocated hypocenter catalogue [Bourne et al., 2014].

### **Inclusion criteria and quality control**

Events were selected for relocation only when they satisfied the Geiger adaptive damping minimum pick requirements [Nakamichi et al., 2014], specifically a minimum of three independent P picks and the network's baseline total-pick threshold. Initial GAD solutions returning root-mean-square travel-time residuals greater than 0.20 s were flagged for manual review and repicking; repicking prioritized improving high-quality P arrivals, adding clear S picks where possible, and reconciling mislabelled or time-shifted arrivals. When repicking failed to reduce residuals below the acceptance threshold, the event was excluded from the relocated catalogue.

Quality control followed an explicit and reproducible workflow. Automated checks verified station-code consistency with the metadata table, removed duplicate or implausible picks, and enforced minimum azimuthal coverage to ensure stable location geometry. Manual inspection then evaluated pick coherency across the network and applied discrete quality flags to derive per-pick weights for the GAD inversion. Final solutions were retained only when they achieved  $\text{RMS} \leq 0.20$  s and met secondary diagnostics, including realistic depth bounds, acceptable formal location uncertainties, and the absence of gross travel-time outliers in the residual distribution.

Robustness and sensitivity of the retained catalogue were assessed through jackknife and bootstrap resampling, velocity model perturbations, and propagation of pick-quality weights to derive realistic uncertainty estimates for hypocenters. The final vetted catalogue, with associated quality metrics, is provided in Table S3 to ensure transparency and enable reuse in hazard and process studies.

### **Data provenance and availability**

Raw seismic waveforms analyzed in this study are owned by the Center for Volcanology and Geological Hazard Mitigation (PVMBG) and subject to PVMBG's data-sharing policy. Processed products – including arrival lists, GAD input/output files, relocated hypocenter catalogue, pick-quality flags, and metadata tables – are provided as Supplementary Material. Full data packages and reproducible scripts are archived and available from the corresponding author or directly from PVMBG upon request, subject to PVMBG's access conditions.

## Methods

### Seismic wave types and properties

Seismic waves are elastic disturbances that propagate through Earth materials and generate time-varying strain and particle motion [Yang, 2014]. These disturbances result from an interaction between the initiating force and the medium's elastic restoring stresses, producing oscillatory motion that can be decomposed into longitudinal (compressional) and transverse (shear) components. Many seismic phases are combinations of these fundamental modes, each with distinct propagation speed, attenuation behaviour, frequency content, and implications for observed ground motion at the surface.

Body waves travel through Earth's interior and carry information about subsurface structure [Zhang, 2016]. Primary (P) waves are compressional, with particle motion parallel to wave propagation; they travel fastest and are the first arriving phase at seismic stations. Secondary (S) waves are shear, with particle motion perpendicular to propagation; they do not travel through fluids and therefore provide complementary constraints on rigidity and the presence of melts or fluids [Shayakhmetov et al., 2023]. Relative arrival times and amplitude decay of P and S phases are primary observables for hypocentre determination and local velocity-model calibration.

Surface waves propagate along the Earth's free surface and typically dominate ground motion at longer periods and larger epicentral distances [Bowden, Tsai, 2017]. Rayleigh waves involve retrograde elliptical particle motion in the vertical plane and sample both near-surface compressional and shear properties, making them sensitive to crustal shear-wave structure [Marghany, 2021]. Love waves are horizontally polarized shear waves trapped near the surface and are especially sensitive to lateral and vertical contrasts in shear velocity [Zhang et al., 2021]. Surface-wave dispersion and attenuation provide independent constraints on shallow structure that complement body-wave location analyses.

### Volcanic versus tectonic seismicity and classification

Earthquakes can be broadly classified by their causative mechanisms into tectonic and volcanic events [Van Der et al., 2022]. Tectonic earthquakes arise from brittle failure on faults driven by regional stress fields, whereas volcanic earthquakes are primarily driven by transient processes related to magmatic and hydrothermal systems: magma ascent, pressurization and depressurization of fluid phases, fracturing induced by volatile exsolution, and conduit or dome collapse. Volcanic seismicity commonly exhibits emergent onsets, low signal-to-noise ratios, and a prevalence of shallow focal depths, all of which complicate phase picking and location [Manzo et al., 2024].

Volcanic earthquakes are often categorised by their waveform and spectral characteristics into families such as deep volcanic, shallow volcanic, hybrid, low-frequency (LP), volcano-tectonic (VT), tremor, and long-period (LP) events. Deep volcanic events typically originate beneath the edifice at depths greater than a few kilometres and are commonly associated with magma movement at depth, whereas shallow volcanic events occur within the uppermost crust (commonly within ~0–2 km beneath the surface) and frequently reflect near-surface fracturing or hydrothermal interactions [Kulhanek, 2002]. Hybrid events combine impulsive high-frequency and emergent low-frequency energy and often indicate fluid-rock interactions. Continuous tremor and LP signals are generally associated with resonant or sustained fluid flow in conduits or hydrothermal fractures; their presence and spectral content are key indicators of changes in pressurization and flow regimes.

An earthquake's hypocentre (focus) is its subsurface point of origin where rupture or the source process initiates [Jain, 2014]; the epicentre is the surface projection directly above the hypocentre [Lomax et al., 2009]. Depth classification is a standard descriptor

for seismic catalogues and is important for discriminating physical processes and hazard implications. For global tectonic contexts, depth classes are commonly defined as shallow (< 70 km), intermediate (70–300 km), and deep (> 300 km), although volcanic-site studies typically use much finer, site-specific depth ranges to separate near-surface (0–2 km), shallow crustal (2–10 km), and deeper crustal sources depending on the local geology and the instrument network resolution.

Clear and consistent definitions of depth classes, combined with robust uncertainty estimates on depth and horizontal location, are essential when interpreting seismicity beneath volcanoes. Because volcanic events are frequently shallow and emergent, quantifying formal location uncertainties, sensitivity to the velocity model, and station coverage is critical for reliable source discrimination and for translating hypocentre patterns into physical interpretations of magma and fluid migration.

### Geiger method and adaptive damping

The Geiger method locates earthquake hypocenters by iteratively minimizing misfit between observed and theoretical travel times using a least-squares update [Luo et al., 2023]. Input requirements comprise station coordinates, P and S arrival times, and a trial velocity model. Each iteration linearizes the travel-time problem about the current hypocenter and origin-time estimate and computes corrective updates to reduce travel-time residuals, thereby closing the gap between observed and calculated arrival times.

For an observation  $i$  the travel-time residual  $r_i$  is the difference between the observed arrival time  $t_{obs,i}$  and the calculated travel time  $t_{calc,i}$  for the current model. Linearizing  $t_{calc,i}$  with respect to small perturbations in origin time and hypocentre coordinates yields the standard Gauss–Newton form. In compact notation, the residual is expressed as

$$r_i \approx \frac{\partial t}{\partial x_i} \Delta x + \frac{\partial t}{\partial y_i} \Delta y + \frac{\partial t}{\partial z_i} \Delta z + \Delta t$$

where,  $\Delta x, \Delta y, \Delta z$  are coordinate corrections and  $\Delta t$  is the origin-time correction. The partial derivatives  $\partial t / \partial x_i$  form the Jacobian matrix  $G$  and are evaluated using ray-path geometry for the adopted velocity model. These derivatives quantify the sensitivity of each pick to changes in hypocentre and origin time and are central to computing robust updates [Brocher, 2008].

The linearized system is written as  $G \Delta m = d$ , where  $\Delta m$  is the vector of parameter updates  $(\Delta x, \Delta y, \Delta z, \Delta t)$  and  $d$  contains the travel-time residuals. To stabilise inversion in the presence of limited azimuthal coverage, emergent phases, or velocity-model uncertainty, the system is solved in damped least-squares form:

$$(G^T G + \lambda I) \Delta m = G^T d,$$

where,  $\Delta \lambda$  is the damping parameter and  $I$  is the identity matrix. Adaptive damping adjusts  $\Delta \lambda$  between iterations to balance fit and model stability: reducing  $\Delta \lambda$  when updates yield consistent residual reductions and increasing  $\Delta \lambda$  when updates produce non-physical parameter jumps. This Geiger adaptive damping (GAD) approach improves convergence and yields more stable hypocentre clouds in sparse or noisy volcanic networks [Lienert et al., 1986].

### Implementation and convergence criteria

Practical implementation requires careful weighting of picks according to quality, per-pick uncertainties, and station geometry. We propagate pick weights into the normal equations by multiplying each row of  $G$  and corresponding residual by the square root of the weight. Iterations proceed until both the maximum parameter update  $|\Delta m|$  and the RMS residual change fall below predefined tolerances or until a maximum number of

iterations is reached. Post-inversion diagnostics include residual histograms, azimuthal gap checks, formal covariance estimates derived from  $(\mathbf{G}^T\mathbf{G} + \lambda\mathbf{I})^{-1}$ , and sensitivity tests that perturb the velocity model or omit individual stations to assess robustness [Diaz, 2016].

Time-frequency transforms such as the S-transform are used to characterise signal content, guide manual picking, and separate overlapping phases prior to location. The S-transform provides a time-localized spectral representation that preserves phase information and scales adaptively with frequency, improving identification of emergent P and S onsets in noisy volcanic records. Reliable picks informed by time-frequency analysis reduce systematic errors in G and d, thereby improving the fidelity and interpretability of GAD relocations [Zhang, 2016].

## Results

### Event counts and classification

Between 01 October 2023 and 30 April 2024 we relocated and vetted 61 volcanic earthquakes that satisfied the GAD inclusion and quality criteria. Events were classified by focal depth into two operational categories chosen to reflect processes relevant to Sinabung monitoring: VTB (shallow volcanic-tectonic), depth < 2.0 km, and VTA (deep volcanic-tectonic), depth  $\geq$  2.0 km. These thresholds were selected to separate near-surface fracturing and hydrothermal interactions from deeper magmatic or plumbing-related sources, consistent with local structural interpretations and the network's vertical resolution (Table 2).

Table 2

Velocity model, resolution tests, and justification

Layer (top–bottom km)	Vp (km s <sup>-1</sup> )	Vs (km s <sup>-1</sup> )	Vertical resolution ( $\Delta z$ , km)	Sensitivity (depth shift for $\pm 10\%$ Vp, km)
0.00–0.50	2.00	1.15	0.2	$\pm 0.05$
0.50–2.00	2.40	1.38	0.3	$\pm 0.10$
2.00–5.00	3.50	2.02	0.6	$\pm 0.25$
5.00–15.00	4.50	2.60	1.0	$\pm 0.50$
>15.00	5.70	3.30	— (poor constraint)	$> \pm 1.0$

Monthly counts and basic summary statistics are presented in Table 3. Across the study interval we identify 34 VTA and 27 VTB events. Temporal behaviour shows that VTA events dominated the early part of the record, while VTB proportions increased during months with elevated near-summit activity; this partitioning suggests alternating periods of deeper source activity and intensified shallow fracturing. We quantified month-to-month variability using Poisson confidence intervals on counts and tested for non-stationarity with a simple  $\chi^2$  test comparing observed monthly counts against a homogeneous Poisson null model; significance and p-values.

Table 3

Classification of earthquake events that occurred on Mount Sinabung †

No	Dates	Amounts	Types of Earthquakes
1	October 2023	6	Deep Earthquake
		7	Shallow earthquake
2	November 2023	2	Deep Earthquake

		6	Shallow earthquake
3	December 2023	6	Deep Earthquake
		3	Shallow earthquake
4	January 2024	6	Deep Earthquake
		8	Shallow earthquake
5	February 2024	4	Deep Earthquake
		1	Shallow earthquake
6	March 2024	4	Deep Earthquake
		0	Shallow earthquake
7	April 2024	6	Deep Earthquake
		2	Shallow earthquake

Each event entry in the catalogue includes event time, geographic coordinates, depth, RMS, number of picks, and formal uncertainty estimates derived from the damped covariance matrix and from station jackknife tests. Classification robustness was assessed by: (1) propagating depth uncertainties to evaluate the fraction of events with depth overlap across the 2.0 km threshold, and (2) performing velocity-model perturbation tests ( $\pm 10\%$   $V_p$ ) to bound systematic depth shifts. Where depth uncertainty caused ambiguous classification, events were flagged in the catalogue and treated separately in aggregated statistics. Reporting these metrics ensures that interpretations linking depth classes to physical processes explicitly account for the limits of the local network and velocity model.

#### **Event catalogue and location quality**

The complete relocated event catalogue is provided in Table 4 and contains UTC origin time, latitude, longitude, depth (km), RMS residual (s), number of picks, pick-quality summary, and formal uncertainty estimates for each entry. Table 4 also lists diagnostic fields used in quality assessment, including azimuthal gap, minimum and maximum station distances, and the per-event covariance trace so readers can reproduce selection thresholds and perform independent filtering.

Accepted locations satisfy a conservative quality threshold of  $RMS \leq 0.20$  s. Events failing to meet this threshold after repicking were excluded from the final catalogue. The typical number of picks per retained event ranged from 4 to 12; events recorded on larger station subsets systematically display lower RMS, reduced formal covariance, and smaller confidence ellipses in horizontal position. To preserve transparency we report both the unweighted and weighted RMS values and provide per-pick weights in the Supplementary files so users may reweight or rerun inversions as required.

Depth sensitivity varies systematically with focal depth and network geometry. Shallow events (-2 km) show relatively stable depth estimates with smaller formal vertical uncertainties under the adopted layered 1-D model, while deeper events exhibit larger vertical shifts under modest velocity perturbations and larger covariance in  $z$ . We quantify this behaviour in S3 by reporting the vertical variance and by providing results from  $\pm 10\%$   $V_p$  perturbation tests and station jackknife runs for each event. For events with depth uncertainties that overlap the VTB/VTA classification threshold, entries are flagged and users are cautioned when attributing physical processes to those particular depths.

Post-processing diagnostics accompany each catalogue entry. These include residual histograms, per-station residual summaries, and azimuthal-coverage metrics that identify events with potentially biased solutions (for example, high azimuthal gap or strongly unequal

station distribution). We include guidance in the README on how to apply additional selection criteria (e.g., minimum number of high-quality picks, maximum azimuthal gap) to produce subsets tailored to specific analyses, such as focal-mechanism studies or fine-scale migration mapping.

Table 4

Relocated event catalogue

Event ID	UTC origin time	Latitude (°N)	Longitude (°E)	Depth (km)	RMS (s)	Number of picks	Pick-quality summary	Covariance trace (km <sup>2</sup> )	Azimuthal gap (°)
EVT_0001	2023-10-03T02:14:12.345Z	3.1712	98.3928	0.45	0.12	8	6H,2M	0.0021	84
EVT_0002	2023-10-07T11:05:47.120Z	3.1698	98.3940	2.35	0.15	6	4H,2M	0.0087	96
EVT_0003	2023-10-15T18:23:09.987Z	3.1745	98.3906	1.10	0.09	10	8H,2M	0.0013	72
EVT_0004	2023-11-01T04:56:33.210Z	3.1669	98.3972	3.80	0.18	7	5H,2M	0.0154	140
EVT_0005	2023-11-20T21:42:02.004Z	3.1720	98.3899	0.20	0.11	9	7H,2M	0.0010	60
EVT_0006	2023-12-05T13:09:58.460Z	3.1704	98.3956	2.90	0.16	5	3H,2M	0.0106	110
EVT_0007	2023-12-18T07:34:21.889Z	3.1758	98.3883	0.85	0.07	12	10H,2M	0.0009	48
EVT_0008	2024-01-09T00:11:44.512Z	3.1685	98.4001	4.50	0.20	6	4H,2M	0.0217	160
EVT_0009	2024-02-02T15:28:30.333Z	3.1733	98.3915	1.75	0.13	8	6H,2M	0.0038	82
EVT_0010	2024-02-	3.16	98.3	2.05	0.14	7	5H,2	0.0075	98

Notes:

- Pick-quality summary: H = high quality pick; M = medium quality pick; L = low quality pick.
- Covariance trace reports the trace of the parameter covariance submatrix for spatial coordinates (proxy for combined location uncertainty); units in km<sup>2</sup>.
- Azimuthal gap is the largest back-azimuthal gap in degrees for stations used in the solution.

### Spatial distribution and Cross-sections

Epicentres are tightly clustered around the volcanic edifice, with the majority of events occurring within a radial distance of approximately 0–5 km from the summit (Fig. 2). The plan-view pattern shows a primary concentration on the upper flank and a secondary, more diffuse cluster extending downslope to the north-west, consistent with shallow fracturing and conduit-proximal stress release. Station coverage and topographic shadowing are reported in Table 2 and were considered when interpreting lateral density variations to avoid over-interpreting apparent gaps caused by network geometry.

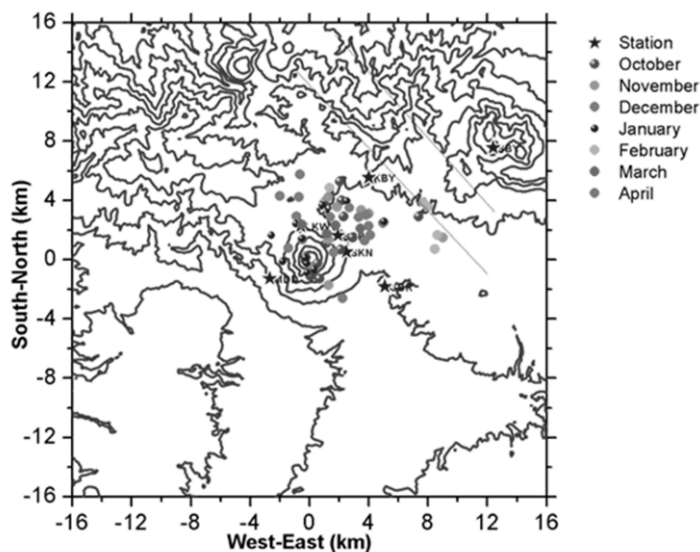


Fig. 2. Distribution of epicenters for October 2023-April 2024 on Mount Sinabung

Orthogonal cross-sections oriented west-east and south-north (Fig. 3a, 3b) delineate two vertically distinct hypocentre populations. Shallow VTB events are concentrated between  $\sim 0.3$  and 2.0 km depth, forming tight, semi-continuous swarms beneath the summit and upper flanks. Their distribution is consistent with near-surface brittle failure or hydrothermal cracking within the edifice. In contrast, deeper VTA events define a separate cluster population between  $\sim 2.5$  and 14 km depth, spatially coherent with deeper conduit structures or mid-crustal magma-transport pathways. Rather than a single point source, the deep population is resolved into several aligned clusters, suggesting vertical segmentation of the plumbing system or the presence of multiple focal zones.

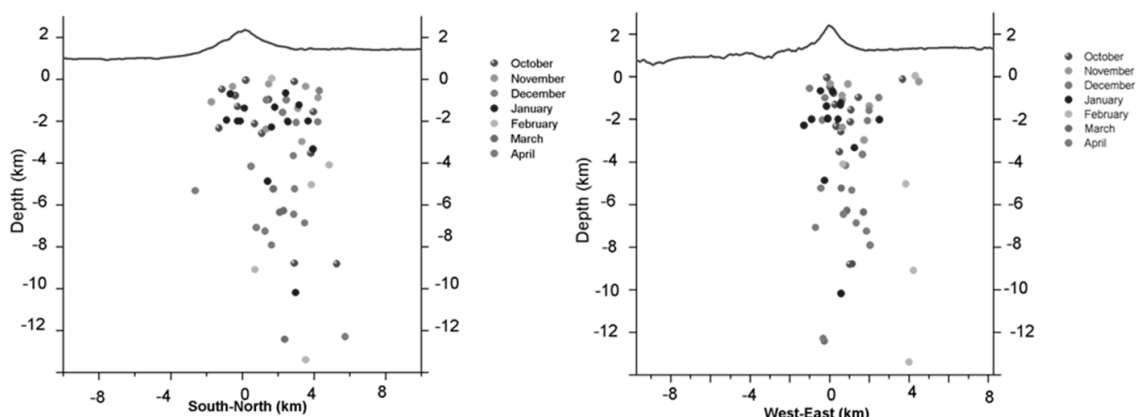


Fig. 3. Distribution of hypocenters recorded between October 2023 and April 2024, shown in orthogonal cross-sections: south-north (a) and west-east (b)

The deepest relocated event in the catalogue occurred in February 2024 at an estimated depth of  $\sim 14$  km: this event is reported with its full uncertainty metrics in Table 3 and was robust to  $\pm 10\%$   $V_p$  perturbation tests and station jackknife runs. Although deeper events exhibit larger formal vertical uncertainties, the February event remained classified as VTA under all sensitivity tests and indicates magmatic or deep crustal processes active beneath the edifice during the study period.

The depth histogram (Fig. 4) exhibits a clear bimodal distribution that matches the operational VTB (shallow) and VTA (deep) classifications. This bimodality supports a two-

tier source model in which shallow, summit-proximal fracturing and deeper, plumbing-related processes operate concurrently but at distinct depths. We quantify the separation by reporting the kernel-density estimate and the fraction of events with overlapping 2 km threshold uncertainty in Table 3; these metrics indicate that the bimodal signature is robust to plausible velocity-model and pick-uncertainty perturbations. Together, plan-view clustering and cross-sectional segmentation provide a consistent structural framework for interpreting magma and fluid migration beneath the volcano.

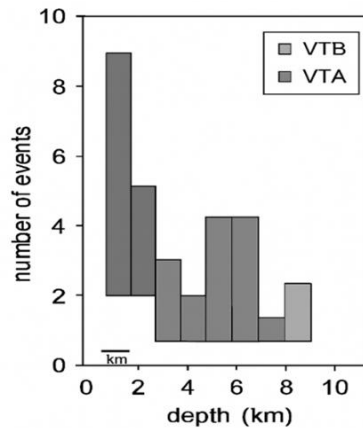


Fig. 4. Distribution of the depth histogram for October 2023–April 2024

### Sensitivity test outcomes

Perturbing the adopted  $V_p$  model by  $\pm 10\%$  yields depth shifts that scale with focal depth: shallow VTB events show shifts typically  $< 1$  km, whereas the deepest VTA events can shift by up to  $\sim 1\text{--}3$  km under these perturbations. Jackknife tests that systematically remove single stations reveal that horizontal location sensitivity increases markedly for events with poor azimuthal coverage; events recorded by six or more stations remain robust, exhibiting only minor positional changes in both horizontal and vertical components. Complementary synthetic experiments and interval-velocity sensitivity analyses indicate that  $V_p/V_s$  and layer thickness trade-offs primarily control vertical resolution and that shallow layers are generally better constrained by the local network than deeper crustal layers.

These outcomes justify the operational depth classification and the conservative quality thresholds applied to the catalogue: events with depth shifts or jackknife-induced relocations that cross the 2.0 km classification boundary are flagged and excluded from depth-sensitive process interpretations. We report per-event sensitivity metrics ( $\pm 10\%$   $V_p$  depth shifts, jackknife displacement statistics, and formal covariance traces) in Table 2 so that readers can independently assess which events are robust for plumbing-system inference and which require cautious interpretation.

## Discussion

### Seismotectonic interpretation and implications

Hypocenter clustering beneath the summit and vertically coherent alignments indicate a segmented magmatic plumbing system at Sinabung. Shallow VTB events ( $\leq 2$  km) reflect brittle failure in a pressurized near-surface hydrothermal or conduit environment, whereas deeper VTA events (to  $\sim 14$  km) delineate fracture networks accommodating magma ascent and stress transfer. The bimodal depth distribution highlights multi-stage storage and intermittent transfer, with phases of deep activity potentially presaging shallow fracturing, enhanced degassing, and elevated eruption probability if pathways become connected.

Local network geometry and velocity-model trade-offs constrain vertical resolution and introduce systematic depth uncertainty; events crossing classification thresholds under  $\pm 10\%$   $V_p$  perturbations or jackknife relocations are therefore interpreted with caution. Strengthening the seismotectonic framework will require denser upper-flank arrays, joint seismic–geodetic inversions, finite-frequency depth refinement, and continuous spectral monitoring to better discriminate brittle failure, fluid resonance, and magmatic intrusion.

### **Comparison with previous studies**

Our relocated hypocenter distribution reproduces the shallow- to mid-crustal bands reported in earlier studies (2016, 2021), with a clear bimodal pattern of shallow VTB events ( $\leq 2$  km) and deeper VTA events extending several kilometres into the mid-crust. The emergence of deeper VTA activity in February 2024 suggests episodic stress-state changes not evident in earlier periods. Absolute depths remain sensitive to the adopted 1-D velocity model and station geometry;  $\pm 10\%$   $V_p$  perturbations and jackknife tests reveal systematic shifts of up to several kilometres for the deepest events. We therefore regard these deepest locations as robust indicators of deep-seated activity but emphasize caution in assigning precise values. Targeted dense-array deployments and joint seismic–geodetic inversions are needed to confirm and refine these depths.

### **Method limitations and monitoring implications**

The principal limitations are the 1-D velocity model and incomplete azimuthal coverage. Geiger linearization presumes small perturbations and depends on initial guesses and travel-time accuracy; adaptive damping stabilizes inversions but cannot eliminate systematic biases. Consequently, depth estimates – especially for the deepest VTA events – carry uncertainties of several kilometres under plausible  $V_p$  perturbations. Covariance and jackknife diagnostics identify which events are robust and which are model-sensitive. To reduce bias and improve depth fidelity, we recommend tomographic or full-waveform inversion using dense local data and incorporating surface-wave and receiver-function constraints.

The relocated hypocenter patterns and monthly event rates have direct operational value for PVMBG. Strategic station densification along NW–SE and NE–SW transects will reduce azimuthal gaps and halve horizontal uncertainties. Routine automated relocations with updated velocity models, accompanied by per-event sensitivity metrics, should be integrated with deformation, gas-flux, and visual observations to detect coupled signals preceding transitions from deep activity to shallow unrest. These measures will strengthen eruption forecasting and provide clearer, evidence-based triggers for alert-level decisions.

## **Conclusions**

Sixty-one volcanic earthquakes were located beneath Mount Sinabung (Oct 2023–Apr 2024): 34 deep VTA events at 2.5–14 km and 27 shallow VTB events at 0.3–2 km.

Epicenters cluster within  $\sim 0$ –5 km of the summit; cross-sections reveal vertically continuous hypocentre pathways consistent with magma-related processes.

Location quality was controlled by RMS thresholding and repicking; sensitivity tests show greater depth uncertainty for deep events due to velocity-model trade-offs.

Recommendations: densify the seismic network to improve azimuthal coverage; refine velocity models via tomography or full-waveform inversion; maintain routine hypocentre relocations to strengthen monitoring and hazard mitigation.

### **Data availability**

Arrival picks (Arrival.dat), station metadata (station.dat), velocity model (Table S2), GAD outputs (Result.dat), and plotting scripts are available from PVMBG Bandung upon reasonable request subject to their data-sharing policy.

## References

1. Gunawan H., Surono, Budianto A., Kristianto et al. Overview of the eruptions of Sinabung Volcano, 2010 and 2013–present and details of the 2013 phreatomagmatic phase. *Journal of Volcanology and Geothermal Research*. 2019. Vol. 382. pp. 103–119. DOI: 10.1016/j.jvolgeores.2017.08.005.
2. Annisa Y., Astriyan G.C., Wahyunia S., Indrastuti N., Massinai M.F.I. Determination of hypocenter using Geiger method in Sinabung Volcano, April–July 2016 period. In: *IOP Conference Series Earth and Environmental Science*. 2021. Vol. 873. No. 1. Art. No. 012007. DOI: 10.1088/1755-1315/873/1/012007.
3. Bakhshian E., Martinez-Pastor B. Evaluating human behaviour during a disaster evacuation process: A literature review. *Journal of Traffic and Transportation Engineering (English Edition)*. 2023. Vol. 10. Issue 4. pp. 485–507. DOI: 10.1016/j.jtte.2023.04.002.
4. Bourne S.J., Oates S.J., Van Elk J., Doornhof D. A seismological model for earthquakes induced by fluid extraction from a subsurface reservoir. *JGR Solid Earth*. 2014. Vol. 119. Issue 12. pp. 8991–9015. DOI: 10.1002/2014JB011663.
5. Bowden D.C., Tsai V.C. Earthquake ground motion amplification for surface waves. *Geophysical Research Letters*. 2017. Vol. 44. No. 1. pp. 121–127. DOI: 10.1002/2016GL071885.
6. Brocher T.M. Key elements of regional seismic velocity models for long period ground motion simulations. *Journal of Seismology*. 2008. Vol. 12. No. 2. pp. 217–221. DOI: 10.1007/s10950-007-9061-3.
7. Charlton T.R. Tertiary evolution of the Eastern Indonesia Collision Complex. *Journal of Asian Earth Sciences*. 2000. Vol. 18. Issue 5. pp. 603–631. DOI: 10.1016/S1367-9120(99)00049-8.
8. Diaz J. On the origin of the signals observed across the seismic spectrum. *Earth-Science Reviews*. 2016. Vol. 161. pp. 224–232. DOI: 10.1016/j.earscirev.2016.07.006.
9. Hariyono E., Liliyasi S. The characteristics of Volcanic Eruption in Indonesia. In: *Volcanoes – geological and geophysical setting, theoretical aspects and numerical modeling, applications to industry and their impact on the human health*. Ed. G. Aiello. InTech. 2018. DOI: 10.5772/intechopen.71449.
10. Jain S. Earthquakes. In: *Fundamentals of Physical Geology*. In: Springer Geology. New Delhi. Springer India. 2014. pp. 337–369. DOI: 10.1007/978-81-322-1539-4\_15.
11. Karasozen E., Karasozen B. Earthquake location methods. *International Journal on Geomathematics*. 2020. Vol. 11. No. 1. Art. No. 13. DOI: 10.1007/s13137-020-00149-9.
12. Katoh S., Iio Y., Nagao H., Katao H., Sawada M., Tomisaka K. SegPhase: development of arrival time picking models for Japan’s seismic network using the hierarchical vision transformer. *Earth Planets Space*. 2025. Vol. 77. Art. No. 118. DOI: 10.1186/s40623-025-02249-y.
13. Kulhanek O. The structure and interpretation of seismograms. In: *International Geophysics*. Vol. 81. Elsevier. 2002. pp. 333–348. DOI: 10.1016/S0074-6142(02)80224-8.
14. Kusumo A.W., Azuma H., Watanabe T., Oda Y. Seismic tomography for subsurface structures imaging beneath Hachijojima Volcanic Island, Izu-Bonin Arc, Japan. *Journal of Seismology*. 2025. Vol. 29. No. 4. pp. 855–873. DOI: 10.1007/s10950-025-10309-9.
15. Lienert B.R., Berg E., Frazer L.N. Hypocenter: An earthquake location method using centered, scaled, and adaptively damped least squares. *Bulletin of the Seismological Society of America*. 1986. Vol. 76. No. 3. pp. 771–783. DOI: 10.1785/BSSA0760030771.
16. Lomax A., Michelini A., Curtis A. Earthquake Location, Direct, Global-Search Methods. In: *Encyclopedia of Complexity and Systems Science*. Ed. R.A. Meyers. New York. NY. Springer New York. 2009. pp. 1–33. DOI: 10.1007/978-3-642-27737-5\_150-2.
17. Luo Z., Shang X., Wang Y., Li X., Liu I.-H., Tai Y. P- and S-wave arrival time combined Bayesian location method for a microseismic event. *Journal of Central South University*. 2023. Vol. 30. No. 11. pp. 3808–3820. DOI: 10.1007/s11771-023-5459-5.
18. Manzo R., Cesca S., Galluzzo D., La Rocca M., Picozzi M., Di Maio R. Source analysis of low frequency seismicity at Mt. Vesuvius by a hybrid moment tensor inversion. *Journal of Volcanology and Geothermal Research*. 2024. Vol. 454. Art. No. 108173. DOI: 10.1016/j.jvolgeores.2024.108173.
19. Marghany M. Wavelet transform and particle swarm optimization algorithms for automatic detection of internal wave from synthetic aperture radar. In: *Nonlinear Ocean Dynamics*. Elsevier. 2021. pp. 247–274. DOI: 10.1016/B978-0-12-820785-7.00005-8.

20. Nakada S., Zaennudin A., Yoshimoto M., Maeno F. et al. Growth process of the lava dome/flow complex at Sinabung Volcano during 2013–2016. *Journal of Volcanology and Geothermal Research*. 2019. Vol. 382. pp. 120–136. DOI: 10.1016/j.jvolgeores.2017.06.012.

21. Nakamichi H., Ukawa M., Sakai S. Precise hypocenter locations of midcrustal low-frequency earthquakes beneath Mt. Fuji, Japan. *Earth, Planets and Space*. 2014. Vol. 56. No. 11. pp. e37–e40. DOI: 10.1186/BF03352542.

22. O’Hara D., Karlstrom L. The arc-scale spatial distribution of volcano erosion implies coupled magmatism and regional climate in the Cascades arc, United States. *Frontiers in Earth Science*. 2023. Vol. 11. Art. No. 1150760. DOI: 10.3389/feart.2023.1150760.

23. Senathirajah K., Bonner M., Schuyler Q., Palanisami T. A disaster risk reduction framework for the new global instrument to end plastic pollution. *Journal of Hazardous Materials*. 2023. Vol. 449. Art. No. 131020. DOI: 10.1016/j.jhazmat.2023.131020.

24. Shayakhmetov S.B., Kalpenova Z.D., Lesov K.S., Umarov Kh.K. Rayleigh and love surface waves with regard to seismic stress state of earth bed. *E3S Web of Conferences*. 2023. Vol. 401. Art. No. 01077. DOI: 10.1051/e3sconf/202340101077.

25. Sutawidjaja I.S., Prambada O., Siregar D.A. The August 2010 Phreatic Eruption of Mount Sinabung, North Sumatra. *Indonesian Journal on Geoscience*. 2013. Vol. 8. No. 1. pp. 55–61. DOI: 10.17014/ijog.8.1.55-61.

26. Van Der Laat L., Mora M.M., Fco. Pacheco J., Lesage P., Meneses E. Seismicity during the recent activity (2009–2020) of Turrialba volcano, Costa Rica. *Journal of Volcanology and Geothermal Research*. 2022. Vol. 431. Art. No. 107651. DOI: 10.1016/j.jvolgeores.2022.107651.

27. Yang W. From Elastic Waves to Seismic Waves. In: *Reflection Seismology*. Elsevier. 2014. pp. 47–81. DOI: 10.1016/B978-0-12-409538-0.00003-8.

28. Zhang Y., Wang T., Bian Y., Yang Q. Features of different types of seismic events in China’s Capital Region. *Earthquake Science*. 2021. Vol. 34. No. 6. pp. 489–506. DOI: 10.29382/eqs-2021-0035.

29. Zhang Z.-X. Stress Waves. In: *Rock Fracture and Blasting*. Elsevier. 2016. pp. 1–36. DOI: 10.1016/B978-0-12-802688-5.00001-4.